

1  
2  
3  
4  
5  
6  
7  
8  
9  
10  
11  
12  
13  
14  
15  
16

## Impacts of Emergent Vegetation on Hyporheic Exchange

S. Huang<sup>1,2</sup>, and J. Q. Yang<sup>1,2</sup>

<sup>1</sup> Saint Anthony Falls Laboratory, University of Minnesota, Minneapolis, MN 55414.

<sup>2</sup> Department of Civil, Environmental, and Geo-Engineering, University of Minnesota, Minneapolis, MN 55455.

Corresponding author: J. Q. Yang ([judyang@umn.edu](mailto:judyang@umn.edu))

### Key Points:

- Emergent vegetation increases the exchange of solutes between surface and subsurface water in the hyporheic zone.
- Vegetation-induced hyporheic exchange can be characterized by the first-order equations with an effective hyporheic exchange velocity.
- The effective velocity of the vegetation-induced hyporheic exchange scale as the total near-bed turbulent kinetic energy  $k_t$ .

## 17 Abstract

18 Hyporheic exchange, or the exchange of water and solutes between surface and subsurface water  
19 at the sediment-water interface, regulates water quality and biogeochemical cycles in aquatic  
20 ecosystems. Vegetation, which is ubiquitous in nature, is known to impact hyporheic exchange,  
21 yet how vegetation impacts hyporheic exchange remains to be characterized. Here, we show that  
22 at the same spatially and temporally averaged flow velocity  $U$ , vegetation increases the rate of  
23 hyporheic exchange by a factor of four. By tracking the movement of fluorescent dye in a flume  
24 with index-matched sediment and translucent vegetation dowels, we demonstrate that vegetation-  
25 induced hyporheic exchange at the sediment-water interface can be characterized by an effective  
26 hyporheic exchange velocity,  $V_H$ . We further demonstrate that  $V_H$  could correlate with the total  
27 near-bed turbulent kinetic energy  $k_t$  rather than mean flow velocity  $U$  when  $k_t < 6 \times 10^{-4} \text{ m}^2/\text{s}^2$ .  
28 A  $k_t$ -based model was developed to characterize the impacts of vegetation on hyporheic  
29 exchange.

## 30 Plain Language Summary

31 The exchange of contaminants and nutrients between surface- and subsurface-water in the  
32 hyporheic zone of rivers and wetlands controls water quality as well as the metabolism of benthic  
33 microbes and the associated biogeochemical cycles. Vegetation, which is ubiquitous in aquatic  
34 ecosystems, has been found to affect the surface- and subsurface-exchange and as such impact  
35 water quality and stream biogeochemical cycles. However, how vegetation impacts this exchange  
36 remains unclear, making it difficult to predict the contaminant transport and biogeochemical cycles  
37 in streams, lakes, and coastal areas with vegetation. In this study, we directly visualized the release  
38 of fluorescent dye from the transparent sediment into the surface water in a water-recirculating  
39 tank filled with translucent vegetation. We discovered that vegetation can significantly increase  
40 the exchange in the hyporheic zone. Furthermore, we proposed a model to predict the impacts of  
41 the vegetation on hyporheic exchange. We believe this finding will help improve predictions of  
42 contaminant transport and biogeochemical cycles in streams and other aquatic ecosystems. The  
43 results of this study will also help ecologists design stream restoration projects that use vegetation  
44 to increase the retention and degradation of contaminants in sediment.

## 45 1 Introduction

46 Hyporheic zone is often referred to the region of saturated sediments underneath the surface  
47 water of a stream, where water, gases, nutrients, and contaminants are consistently being  
48 exchanged (Boano et al., 2014; Boulton et al., 1998; Gooseff, 2010). The exchange between  
49 surface and subsurface water supplies nutrients and oxygen to underground microbes and as such  
50 controls the biogeochemical cycles and biodiversity of stream bed (Battin et al., 2008; Jones Jr &  
51 Holmes, 1996; Tonina & Buffington, 2009; Wohl, 2016). The exchange in hyporheic zone also  
52 determines the retention and degradation of contaminants in stream (Grant et al., 2014;  
53 Lewandowski et al., 2011; McCallum et al., 2020). Fundamental understanding of the exchange  
54 in hyporheic zone is critical for predicting the biogeochemical cycles, biodiversity, and fate of  
55 contaminants in streams.

56 Over the past decades, extensive studies have been conducted to characterize the impacts  
57 of channel morphology such as bedforms (Buffington & Tonina, 2009; Dudunake et al., 2020;  
58 Marion et al., 2002; Packman et al., 2004; Tonina & Buffington, 2007) and sinuosity of river  
59 (Boano et al., 2006; Cardenas, 2009) on hyporheic exchange. Recent field studies show that the

60 presence of vegetation in stream increases the in-stream transient storage controlled by hyporheic  
 61 exchange (Ensign & Doyle, 2005; Salehin et al., 2003). However, the impact of in-channel aquatic  
 62 vegetation on the hyporheic exchange has not been systematically quantified (Ding et al., 2020).

63 In-channel aquatic vegetation exerts drag on the surface flow (Cheng & Nguyen, 2011;  
 64 D'Ippolito et al., 2019), which creates spatial heterogeneities in near-bed mean flow velocity (Zhao  
 65 & Fan, 2019), shear stress (Salvador et al., 2007; Yang et al., 2015), turbulent kinetic energy (Xu  
 66 & Nepf, 2020), and pressure (Nepf & Koch, 1999; Yuan et al., 2021). In addition, vegetation drag  
 67 also extracts energy from the mean flow and converts it to turbulent kinetic energy  $k_t$  (Nepf, 1999,  
 68 2012; Tanino & Nepf, 2008). Both spatial heterogeneity in hydraulic head (Boano et al., 2014; Lee  
 69 et al., 2022; Shen et al., 2020; Tonina & Buffington, 2007; Yuan et al., 2021) and turbulence  
 70 (Roche et al., 2018; Roche et al., 2019; Rousseau & Ancey, 2020; Voermans et al., 2017;  
 71 Voermans et al., 2018b) are known to induce hyporheic exchange. Therefore, we anticipate that  
 72 the drag exerted by vegetation, which induces spatial hydraulic gradient and turbulence, can induce  
 73 hyporheic exchange.

74 The goal of this study is to quantify the impact of emergent vegetation, i.e., plants that  
 75 extend out of the water surface, on hyporheic exchange across the sediment-water interface in  
 76 streams with a flat gravel bed through systematically controlled laboratory experiments. We  
 77 conducted a series of dye-visualization experiments in a water-recirculating flume filled with  
 78 transparent hydrogel beads that simulate a gravel bed and acrylic cylinders that simulate emergent  
 79 vegetation stems. We used an effective hyporheic exchange velocity,  $V_H$ , to characterize the  
 80 exchange rate of fluorescent dye between surface and subsurface water in the hyporheic zone. In  
 81 addition, the mean flow velocities were measured and the near-bed turbulent kinetic energy  $k_t$  was  
 82 calculated. Our experiments show that  $V_H$  in channels with emergent vegetation scales with  $k_t$   
 83 when  $k_t < 6 \times 10^{-4} \text{ m}^2/\text{s}^2$ , because  $k_t$  reflects the vegetation-drag-induced near-bed turbulence  
 84 and spatial heterogeneity in hydraulic head, both of which drive hyporheic exchange.

## 85 2 Theories

### 86 2.1 Pseudo-first-order equations for hyporheic exchange

87 Here, we use pseudo-first-order equations (Wu et al., 2001) to quantify the impacts of the  
 88 vegetation on the rate of solute exchange across the sediment-water interface. We hypothesized  
 89 that Fick's first law governs the vertical hyporheic flux in vegetated channels with gravel flat beds,  
 90 like the gas diffusion across a diffusive boundary layer. Thus, similar to gas transfer model based  
 91 on the thin-film theory (Jørgensen & Revsbech, 1985; O'Connor & Hondzo, 2008), the rate of  
 92 hyporheic exchange can be quantified by an effective hyporheic exchange velocity  $V_H$ . Note that  
 93 here we focus on the hyporheic exchange between the surface water and the top sediment layers.  
 94 We do not consider the variation in diffusivity with depth within deeper sediment as discussed in  
 95 Chandler et al. (2016) and the longitudinal dispersion discussed in Bottacin-Busolin (2017). Below  
 96 we describe how we use  $V_H$  and the pseudo-first-order equations to predict the release of solutes  
 97 from the pore water of the top sediment layers to the surface water in a recirculating flume. In  
 98 Section 3, we describe how we use flume experiments to validate the model.

99 First, at the beginning of the experiment, a solute is uniformly distributed in the pore space  
 100 of the top several layers of sediment with concentration  $C_s$ . Due to hyporheic exchange, the solute  
 101 in the sediment is transported into the surface water through a mixing layer, such that  $C_s$  decreases  
 102 with time  $t$ . Once solute leaves the sediment bed, it is quickly mixed with the surface water with

103 a uniform concentration  $C_w$ . For simplicity, we assume that the solute concentrations in the top  
 104 sediment layers and in surface water are both uniformly distributed, with volume  $V_{ol,s}$  and  $V_{ol,w}$ ,  
 105 respectively. We hypothesize that the exchange between surface and subsurface water at the  
 106 sediment-water interface can be characterized by a pair of pseudo-first-order equations with an  
 107 effective hyporheic exchange velocity  $V_H$ . Therefore, based on mass balance between the surface  
 108 water and subsurface water:

$$\frac{dC_s}{dt} = -V_H \frac{A_{SWI}\phi_s}{V_{ol,s}} (C_s - C_w) \quad (1)$$

$$\frac{dC_w}{dt} = -V_H \frac{A_{SWI}\phi_s}{V_{ol,w}} (C_w - C_s). \quad (2)$$

109 Here  $\phi_s$  is the sediment porosity;  $A_{SWI}$  is the horizontal area of the sediment-water  
 110 interface ( $m^2$ ), and  $V_H$  is the effective hyporheic exchange velocity (m/s), which is defined as  
 111  $V_H = D_e/\delta_D$ .  $D_e$  is the effective diffusion coefficient ( $m^2/s$ ) and  $\delta_D$  is the mixing layer thickness  
 112 (m). If the solute concentration in the surface water is negligible ( $C_s \gg C_w$ ), the analytical solution  
 113 of Eq. 1 is  $C_s(t) = C_{s0}e^{-V_H A_{SWI}\phi_s t/V_{ol,s}}$ , which predicts an exponential decrease in the solute  
 114 concentration in the pore space of the sediment. Here  $C_{s0}$  indicates the initial solute concentration  
 115 in the sediment. The schematic diagram of the proposed model is shown in Fig. S1 in the  
 116 Supplementary Information. The fitting of this model (Eqs. 1 and 2) to our experimental results  
 117 are discussed in Section 4.1. Note that effective diffusion coefficient  $D_e$  was defined differently  
 118 using 1-D diffusion equation in other studies (Chandler et al., 2016; Grant et al., 2012; O'Connor  
 119 & Harvey, 2008). Comparisons of the  $D_e$  based on their definition is discussed in Section 4.1.

## 120 2.2 Impact of emergent vegetation on hyporheic exchange

121 In-channel vegetation exerts drag on surface flow (Cheng & Nguyen, 2011; D'Ippolito et  
 122 al., 2019) and converts kinetic energy of the mean flow to turbulent kinetic energy (Nepf, 1999;  
 123 Tanino & Nepf, 2008). The drag force generated by vegetation can be expressed as follows (Cheng  
 124 & Nguyen, 2011),

$$F_D = \frac{1}{2} a V_{ol,v} C_D \rho_w U^2 \quad (3)$$

125 Here  $a$  is the frontal area per unit volume ( $m^{-1}$ ) which can be estimated as  $a = n d_v$  for cylindrical  
 126 vegetation (Yang & Nepf, 2018);  $n$  is the stem density (stem/ $m^2$ );  $d_v$  is the diameter of model  
 127 vegetation stem (m);  $C_D$  is the drag coefficient of the vegetation;  $V_{ol,v}$  is the volume of water with  
 128 vegetation canopy ( $m^3$ );  $\rho_w$  is fluid density ( $kg/m^3$ ), and  $U$  is the flow velocity (m/s). The drag  
 129 exerted by the emergent vegetation generates spatial heterogeneities in the near-bed mean flow  
 130 velocity, and further generated the hydraulic head that induces the hyporheic exchange (Yuan et  
 131 al., 2021). In addition, the vegetation-generated turbulent kinetic energy  $k_{tv}$  can be estimated by  
 132 the energy extracted from the mean flow due to vegetation drag (Tanino & Nepf, 2008; Yang et  
 133 al., 2016):

$$k_{tv} = 1.2 \left[ C_D \frac{\phi_v}{(1 - \phi_v) \pi/2} \right]^{2/3} U^2. \quad (4)$$

134 Here  $\phi_v$  is the solid fraction of the vegetation. For cylindrical dowels,  $\phi_v = \pi a d_v/4$  (Yang &  
 135 Nepf, 2018). The total near-bed turbulent kinetic energy  $k_t$  then can be approximated as the sum  
 136 of bed-generated  $k_{tb}$  and vegetation-generated  $k_{tv}$  (Yang et al., 2016; Yang & Nepf, 2018, 2019),

$$k_t = k_{tb} + k_{tv}. \quad (5)$$

137 Here  $k_{tb} = C_f U^2 / 0.19$ ;  $C_f$  is bed drag coefficient. The vegetation generated turbulence is a result  
 138 of vegetation drag and as thus correlates with the spatial heterogeneity in hydraulic head which is  
 139 also induced by vegetation drag. We hypothesis that near-bed turbulent kinetic energy  $k_t$  reflects  
 140 the compound effect of vegetation-drag-induced spatial heterogeneity in near-bed hydraulic head  
 141 and near-bed turbulence on hyporheic exchange and thus  $k_t$  can be applied to predict the  
 142 vegetation-induced hyporheic exchange.

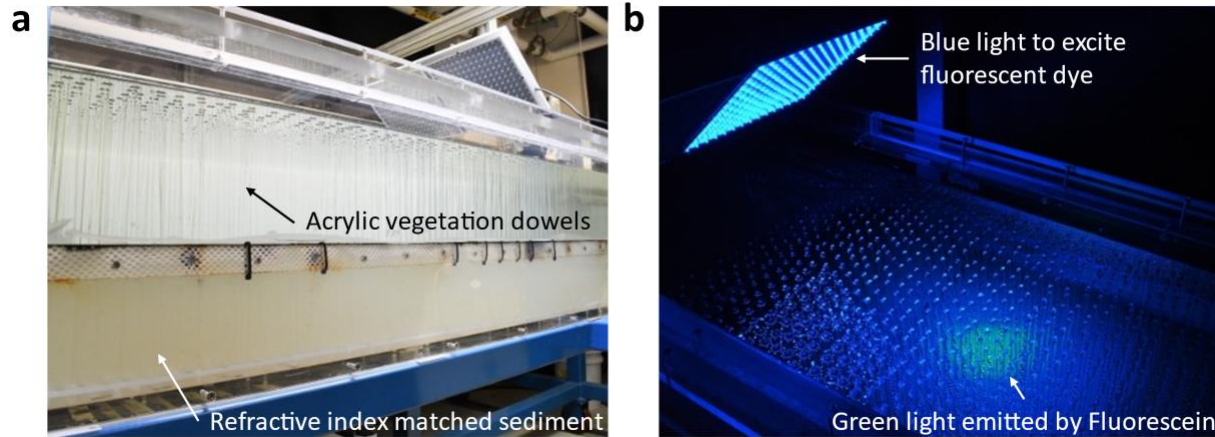
### 143 3 Materials and Methods

#### 144 3.1 Experimental setup

145 Hyporheic exchange experiments were conducted in a horizontal race-track flume at the  
 146 University of Minnesota's St. Anthony Falls Laboratory. The flume is 14-m-long and 60-cm-wide  
 147 and has a 150-cm-long by 60-cm-wide straight test section (Figs. 1 and S2). The water depth in all  
 148 experiments was  $20.0 \pm 0.1$  cm. The flow in the flume was driven by a propeller. The flow velocity  
 149 was directly measured by a side-looking Acoustic Doppler Velocimeter (Nortek Vectrino,  
 150 Norway, Fig. S5).

151 The bottom of the test section (60 cm  $\times$  150 cm) was removed, and the space underneath  
 152 was filled with transparent hydrogel beads ( $5.6 \pm 0.6$  mm in diameter) to simulate a gravel bed.  
 153 Method to make the hydrogel beads developed by Ma et al. (2019) is described in Text S1 in the  
 154 Supplementary Information. To keep the hydrogel beads in place and the sediment bed flat, a black  
 155 polyester mesh (4 mm pore size) was placed on the top of the beads. While the bed was mostly flat  
 156 without obvious bedform, one of the downstream corners of the mesh tilted and formed a small  
 157 lateral slop of 1/150 and 1/60 in streamwise direction and spanwise direction, respectively. This  
 158 structure was roughly the same in both cases with and without vegetation. We anticipate this small  
 159 structure would not affect our results, because we focus on the difference in hyporheic exchange  
 160 between channels with and without vegetation.

161 To investigate the impact of rigid emergent vegetation on the flow, the translucent and  
 162 cylindrical acrylic dowels with  $d_v = 6.4 \pm 0.1$  mm diameter were inserted in a staggered pattern  
 163 (Fig. S5) on a PVC board fixed under the sediments. The dowels extended through the whole water  
 164 column and entire sediment depth. The solid volume fraction of vegetation  $\phi_v$  in this study is 0.05,  
 165 in the range of typical values found in marshes (Nepf, 2012; Yang et al., 2016). The stem density  
 166  $n$  is 1,514 stems/m<sup>2</sup>, and the spanwise center-to-center distance between two dowels  $2ds$  is 2.6  
 167 cm (Fig. S5). The vegetation frontal area per unit canopy volume  $a = nd$  is  $9.8 \text{ m}^{-1}$ . There are  
 168 1,363 dowls in the test section. In the area where images were processed, there were 47 dowels.



169

170 **Figure 1.** Experiments in a recirculating flume to visualize the exchange of fluorescent dye  
 171 between surface and subsurface water. Refractive-index-matched sediment and translucent  
 172 vegetation dowels were used. Green, fluorescent dye was injected into the sediment and a blue  
 173 lamp was used to excite the dye.

174 Instantaneous flow velocity was measured using a side-looking Acoustic Doppler  
 175 Velocimeter (ADV; Nortek Vectrino, Norway) mounted on a 2-D moving system with 200 Hz  
 176 sampling rate for 2.5 minutes. Solid glass beads with specific gravity 2.6 and mean diameter 35  
 177 micrometers (3000 E-Spheriglass; Potters Industries Inc., Pennsylvania) were added to the water  
 178 as seeding particles. Measurements with signal-to-noise ratio below 15 dB were removed from  
 179 data analysis. A bivariate kernel density function was used to remove noise signals from velocity  
 180 measurements (Islam & Zhu, 2013). For cases with vegetation, three dowels were removed to  
 181 make space for the probe of the ADV. We anticipate that the ADV probe would not affect the  
 182 velocity measurements, because the probe was 5 cm away from the measurement location (Fig.  
 183 S5). Four velocity profiles were measured at the middle of test section to estimate spatial-weighted  
 184 averaged velocities for each case. For cases without vegetation, profiles were 5, 13, 22, 30 cm  
 185 away from the side wall, respectively. The measured locations and weighted average method for  
 186 cases with vegetation can be found in Fig. S5.

187 The spatially averaged near-bed turbulent kinetic energy  $k_t$  was calculated from the  
 188 instantaneous flow velocity measured 2 cm above the bed at the four representative locations using  
 189 an ADV. Specifically, the local  $k_t$  at each location was calculated as  $(\overline{u'^2} + \overline{v'^2} + \overline{w'^2})/2$ . Here  
 190  $u'$ ,  $v'$ , and  $w'$  are flow velocity fluctuations in streamwise, spanwise, and vertical direction,  
 191 respectively. The spatially averaged near-bed  $k_t$  was calculated using a spatial-average method  
 192 justified in Yang et al. (2015) from local  $k_t$  at 4 locations as shown in Fig. S5. Location at 2 cm  
 193 above bed was chosen because within 2 cm from the bed the sampling volume of the ADV is  
 194 interfered by the boundary such that the signal-to-noise ratio became smaller than 15 dB. Previous  
 195 studies using same model vegetation show that the vertical distribution of turbulent kinetic energy  
 196 is uniform above a thin boundary layer (Nepf, 1999; Yang et al., 2015), thus, our measurement of  
 197  $k_t$  at 2 cm above the bed captures the impacts of vegetation on near-bed turbulent kinetic energy.

## 198 3.2 Fluorescent dye release experiments

199 Fluorescent dye release experiments were conducted to measure the rate of hyporheic  
200 exchange. First, dye solution was prepared by adding fluorescein sodium salt (Sigma-Aldrich  
201 F6377) to DI water at 0.002‰ weight ratio. The water depth in the flume was adjusted to  $20.0 \pm$   
202  $0.1$  cm. The fluorescent dye was injected into a  $44 \text{ cm} \times 43 \text{ cm}$  sediment area up to 5 cm deep  
203 (accumulative dye concentration is  $(1.286 \pm 0.006) \times 10^{-3} \text{ mg/cm}^2$ ) using a peristaltic pump (L/S  
204 7550-50; Masterflex, Germany). The flow was stopped during the injection. The amount of dye  
205 injected at each location was monitored by a scale during the injection process to make sure the  
206 uniformly distribution of dye within the injection area. The dye emits green light at 520-nm  
207 wavelength, when it is excited by blue light at 490-nm wavelength (Osenbroch et al., 2005). The  
208 fluorescence intensity detected by downward-looking camera were calibrated against the dye  
209 concentration in the sediment (Text S2 and Fig. S6 in the Supplementary Information). Our  
210 measurements indicate that the fluorescence intensity is linearly proportional to the accumulative  
211 dye concentration, i.e., mass per unit area (Fig. S6a). The picture of injection equipment and  
212 injection locations can be found in Figs. S7-S8.

213 One square lamp ( $30 \text{ cm} \times 30 \text{ cm}$ ) with blue LED arrays were placed at the center of the  
214 channel and 33 cm above the water surface. The angle between lamp and ground was  $40^\circ$ . The  
215 light emitted from the dye was passed through a green light filter (FGV9S; Thorlabs, Newton) and  
216 captured by a downward-looking industrial camera (BFS-U3-16S2C-CS; FLIR Systems,  
217 Wilsonville) with a 6 mm focal length lens (ArduCAM, China) placed 120 cm above the sediment  
218 bed. Afterwards, flow was recirculated in the flume using a propeller, and the fluorescence  
219 intensity within the sediment bed was monitored every 5 minutes for a 16.6-hour duration. The  
220 unsteady period of flow development at the beginning of the experiment is relatively short (few  
221 minutes) compared to the time scale of whole experiment ( $> 16.6$  hours) and the data at early stage  
222 was not included in the model fits (Text S3 in the Supplementary Information). Experiments  
223 without vegetation were conducted at mean flow velocities of 1.7, 4.0, 6.6, 15.4 cm/s. Experiments  
224 with vegetation were conducted at flow velocities of 0.7, 1.6, 2.4, 3.6 cm/s. Each case was  
225 conducted twice.

226 The effective hyporheic exchange velocity  $V_H$  was estimated by fitting the numerical  
227 solution of the pseudo-first-order equation (Eq. 1) to the measured fluorescence intensity versus  
228 time (Fig. 2). First, pixels occupied by vegetation and the mesh were removed, and the  
229 fluorescence intensity of the light emitted by the dye in the sediment was estimated by averaging  
230 the image intensity of pixels occupied by the pore space. From the series of images, the curve of  
231 fluorescence intensity versus time, i.e., washout curve, can be obtained. Then, the proposed model  
232 (Eqs. 1-2) were fitted numerically to the measured fluorescence intensity versus time (Fig. 2). The  
233 effective hyporheic exchange velocity  $V_H$  and background image intensity was determined by  
234 minimizing the root mean square error between the measured curve and the simulated curve. The  
235 detail image processing method and fitting procedure can be found in Text S3 and Fig. S10 in the  
236 Supplementary Information.

237 To compare the effective hyporheic exchange velocities  $V_H$  for the cases without and with  
238 vegetation, we conducted the one-way analysis of covariance (ANOCOVA) using ‘aoctool’  
239 function in MATLAB, with  $p$ -value indicating the statistical difference (Philippas, 2014). When  
240  $p < 0.05$ , the difference between two data sets is often considered to be statistically significant.

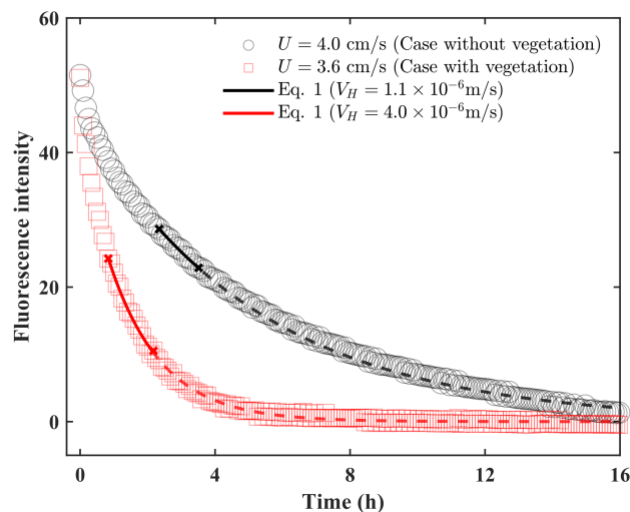
241 Note that once dye leaves the sediment, it is quickly diluted in the surface water. Our  
 242 experiments show that the dye in the surface water, whose concentration is much smaller than the  
 243 dye concentration in the sediment, does not affect the results, i.e., the light captured by the camera  
 244 above the water surface is mainly contributed by the dye in the sediment.

## 245 4 Results

### 246 4.1 Dye release experiments verify the proposed model

247 First, we use dye release experiments described in Section 3.2 to verify the proposed  
 248 hyporheic exchange model (Eqs. 1-2). The fluorescence intensity at different times shows that the  
 249 dye concentration in the sediment bed decreases over time (Fig. S9). The spatially averaged  
 250 fluorescence intensity of the green light emitted by the fluorescent dye was plotted versus time to  
 251 characterize the leaving of dye from the observed area. The method to identify the pixels related  
 252 to the pore space can be found in Text S3 in the Supplementary Information. Fig. 2 shows two  
 253 representative cases without and with vegetation at a similar spatially and temporally averaged  
 254 flow velocity  $U$  measured by an ADV. The decrease in dye concentration occurred much faster in  
 255 a channel with vegetation than in a channel without vegetation, indicating that the presence of  
 256 vegetation increases the hyporheic exchange rate.

257 To capture the rate of exchange, we fit the spatially averaged fluorescence intensity versus  
 258 time measurements with the proposed model (Eqs. 1 and 2) numerically (see Text S3 in the  
 259 Supplementary Information for details). The fitted results (solid curves in Fig. 2) show an  
 260 exponential decrease in fluorescence intensity. The predictions of the model are consistent with  
 261 the data which were not included in the fitting of the effective hyporheic exchange velocity  $V_H$   
 262 (dash lines in Fig. 2), indicating that the proposed model can be used to characterize the hyporheic  
 263 exchange observed in the experiments.



264  
 265 **Figure 2.** The concentration of the fluorescent dye in the sediment, represented by the fluorescence  
 266 intensity of the emitted green light, decays over time. The flow was started at time = 0 hour. The  
 267 black and red symbols represent the fluorescence intensities relative to the background image  
 268 intensities in channels without vegetation and with vegetation of volume fraction  $\phi_v = 0.05$ ,  
 269 respectively, at a similar flow velocity 4 cm/s. The black and red solid curves represent the fits of

270 the measurements with the solution of Eq. 1 with both  $R^2 = 0.99$ . The model fits are conducted  
 271 when the streamwise fluorescence intensity decrease uniformly (see Text S3 in the Supplementary  
 272 Information for details). In the experiments, the horizontal area of the sediment-water interface  
 273  $A_{SWI} = 0.19 \text{ m}^2$ ; the sediment porosity  $\phi_s = 0.3$ ; the volume of pore space in the sediment  
 274  $V_{ol,s} = 1200 \pm 9 \text{ mL}$ , and the volume of surface water  $V_{ol,w} = 2830 \text{ L}$ . The fitted parameters are  
 275  $V_H$  and background image intensity. Dash lines show the model predictions.

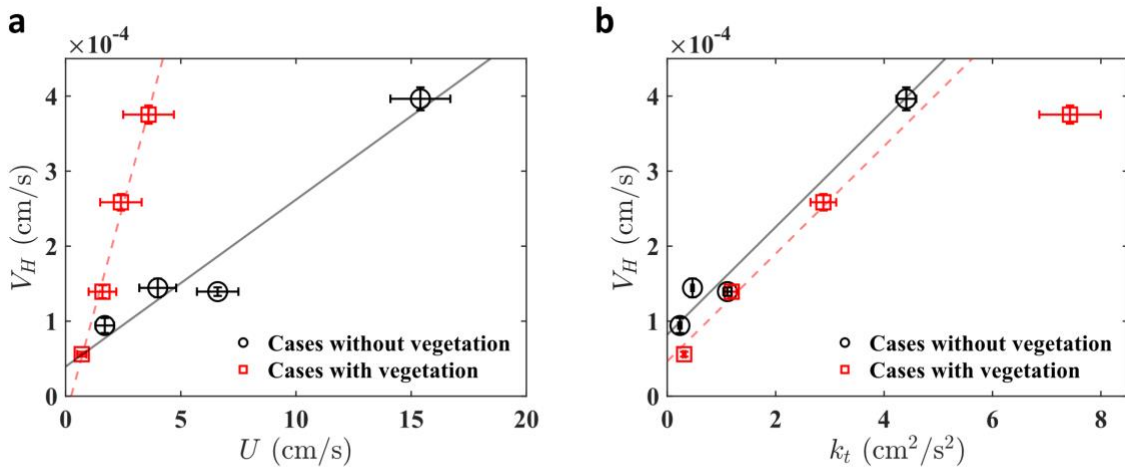
276 Note that in the complementary dye release experiments with a side-looking camera, we  
 277 observed a streamwise elongation of dye plume. The velocity of the dye front is 1.0~1.5% of the  
 278 velocity of overlying flow to the downstream in the sediment, which is not considered in the  
 279 proposed model. On the other hand, the vertical mixing of dye in the sediment was not significant  
 280 compared with the exchange of dye at the sediment-water interface (Text S4 in the Supplementary  
 281 Information).

282 At a similar flow velocity around 4 cm/s, the effective hyporheic exchange velocity  $V_H$  of  
 283 the case without vegetation is  $1.1 \times 10^{-6} \text{ m/s}$ , about 4 times smaller than  $V_H$  of the case with  
 284 vegetation which  $V_H = 4.0 \times 10^{-6} \text{ m/s}$  (Fig. 2). In addition, the slope of regression line of cases  
 285 with vegetation is 4 times higher than the slope of regression line of cases without vegetation (Fig.  
 286 3a). These results indicate that the presence of vegetation increases the rate of hyporheic exchange  
 287 by a factor of 4 at the same mean flow velocity  $U$ .

288 Finally, we provide comparison of our results with pervious study. The effective diffusion  
 289 coefficients  $D_e$  calculated using 1-D diffusion equation in our experiments are provided in Table  
 290 S1 and are compared with the interfacial transport model proposed by Volermans et al. (2018a) in  
 291 Fig. S12 in the Supplementary Information.

#### 292 4.2 The scale of effective hyporheic exchange velocity with turbulent kinetic energy

293 By comparing  $V_H$  versus  $U$  and  $k_t$  for cases without and with vegetation, we exam whether  
 294 the exchange rate at the sediment-water interface is controlled by mean flow velocity or turbulent  
 295 kinetic energy. Based on ANOCOVA (see methods for details), the difference between lines  $V_H$   
 296 versus  $U$  measurements for cases without and with vegetation is statistically significant (with  $p =$   
 297  $0$  smaller than statistical threshold value 0.05). In contrast, at  $k_t < 6 \times 10^{-4} \text{ m}^2/\text{s}^2$ , the  
 298 difference between the slopes of lines  $V_H$  versus  $k_t$  measurements for cases without and with  
 299 vegetation is not significant ( $p = 0.26$ ; Fig. 3b). Note that the intercept of line  $V_H$  versus  $k_t$   
 300 without vegetation is statistically significantly bigger than the intercept of line with vegetation and  
 301  $V_H$  in the vegetated case with  $k_t = 7.4 \times 10^{-4} \text{ m}^2/\text{s}^2$  deviates from the linear fitting for  $k_t <$   
 302  $6 \times 10^{-4} \text{ m}^2/\text{s}^2$ . These deviations are reflections of the complex interactions of flow and  
 303 vegetation, especially at high turbulent conditions. Nevertheless, our results show that compared  
 304 with mean flow velocity, turbulent kinetic energy is a better predictor of hyporheic exchange for  
 305 channels with vegetation, especially at  $k_t < 6 \times 10^{-4} \text{ m}^2/\text{s}^2$ .



306

307 **Figure 3.** (a) The effective hyporheic exchange velocity  $V_H$  versus mean flow velocity  $U$  of cases  
 308 without vegetation (black) and with vegetation of volume fraction  $\phi_v = 0.05$  (red). The black  
 309 solid line ( $y = (0.2x + 0.4) \times 10^{-4}$ ) and red dash line ( $y = (1.1x - 0.3) \times 10^{-4}$ ) represent  
 310 linear fits to measurements without and with vegetation with  $R^2 = 0.89$  and  $R^2 = 0.95$ ,  
 311 respectively. (b)  $V_H$  versus the total near-bed turbulent kinetic energy  $k_t$  of cases without  
 312 vegetation (black) and with vegetation (red). The black solid line ( $y = (7.2x + 8.2) \times 10^{-5}$ ) and  
 313 red dash line ( $y = (7.2x + 4.7) \times 10^{-5}$ ) represent linear fits of the measurements without and  
 314 with vegetation with both  $R^2 = 0.92$ .

## 315 5 Conclusions

316 Vegetation has been acknowledged to enhance the exchange between surface and  
 317 subsurface water in the aquatic habitats, yet the impacts of vegetation on hyporheic exchange have  
 318 not been characterized. Here we propose a model to characterize the vegetation-induced hyporheic  
 319 exchange in channels with vegetation. By conducting tracer experiments using fluorescent dye and  
 320 refractive-index-matched sediment, we show that the vegetation-induced hyporheic exchange at  
 321 the sediment-water interface can be characterized by the pseudo-first-order equations with an  
 322 effective hyporheic exchange velocity  $V_H$ . We demonstrate that at the same spatially and  
 323 temporally averaged flow velocity  $U$ , vegetation increases  $V_H$  by up to a factor of four when  
 324 compared with channels without vegetation. We further demonstrate that  $V_H$  scales with the total  
 325 near-bed turbulent kinetic energy  $k_t$  instead of  $U$  when  $k_t < 6 \times 10^{-4} \text{ m}^2/\text{s}^2$ . The results of the  
 326 proposed hyporheic exchange model will enable quantitative analysis of the impacts of vegetation  
 327 on the exchange of contaminants and nutrients in the hyporheic zone.

## 328 Acknowledgments

329 This study was supported by JQ Yang's startup funds and Minnesota Water Research Fund. The  
 330 authors would like to thank Sam Nguyen for his assistance with the experiments, Peter Kang for  
 331 insightful discussions, and Benjamin Erickson, Erik Steen, and Jeffrey Marr for help with the  
 332 flume.

333 **Data Availability Statement**

334 The raw data of the dye release experiments with a downward-looking camera has been deposited  
 335 in The Data Repository for University of Minnesota (<https://doi.org/10.13020/W282-JJ11>). The  
 336 raw data of the dye release experiments with a side-looking camera and dye calibration have been  
 337 deposited on Zenodo (<https://doi.org/10.5281/zenodo.6412364>).

338 The codes used to process the images and fit the washout curves have been deposited on Zenodo  
 339 (<https://doi.org/10.5281/zenodo.6407198>).

340 **References**

- 341 Battin, T. J., Kaplan, L. A., Findlay, S., Hopkinson, C. S., Marti, E., Packman, A. I., . . . Sabater, F. (2008).  
 342 Biophysical controls on organic carbon fluxes in fluvial networks. *Nature geoscience*, *1*(2), 95-100.
- 343 Boano, F., Camporeale, C., Revelli, R., & Ridolfi, L. (2006). Sinuosity-driven hyporheic exchange in meandering  
 344 rivers. *Geophysical Research Letters*, *33*(18).
- 345 Boano, F., Harvey, J. W., Marion, A., Packman, A. I., Revelli, R., Ridolfi, L., & Wörman, A. (2014). Hyporheic  
 346 flow and transport processes: Mechanisms, models, and biogeochemical implications. *Reviews of*  
 347 *Geophysics*, *52*(4), 603-679.
- 348 Bottacin-Busolin, A. (2017). Non-Fickian dispersion in open-channel flow over a porous bed. *Water Resources*  
 349 *Research*, *53*(8), 7426-7456.
- 350 Boulton, A. J., Findlay, S., Marmonier, P., Stanley, E. H., & Valett, H. M. (1998). The functional significance of the  
 351 hyporheic zone in streams and rivers. *Annual review of Ecology and systematics*, *29*(1), 59-81.
- 352 Buffington, J. M., & Tonina, D. (2009). Hyporheic exchange in mountain rivers II: Effects of channel morphology  
 353 on mechanics, scales, and rates of exchange. *Geography Compass*, *3*(3), 1038-1062.
- 354 Cardenas, M. B. (2009). A model for lateral hyporheic flow based on valley slope and channel sinuosity. *Water*  
 355 *Resources Research*, *45*(1).
- 356 Chandler, I., Guymer, I., Pearson, J., & Van Egmond, R. (2016). Vertical variation of mixing within porous  
 357 sediment beds below turbulent flows. *Water resources research*, *52*(5), 3493-3509.
- 358 Cheng, N.-S., & Nguyen, H. T. (2011). Hydraulic radius for evaluating resistance induced by simulated emergent  
 359 vegetation in open-channel flows. *Journal of hydraulic engineering*, *137*(9), 995-1004.
- 360 Ding, M., Wan, J., Li, Q., & Tang, B. (2020). Literature Review: How in-channel aquatic vegetation (IAV) affects  
 361 hyporheic exchange (HE). IOP Conference Series: Materials Science and Engineering,
- 362 Dudunake, T., Tonina, D., Reeder, W., & Monsalve, A. (2020). Local and Reach-Scale Hyporheic Flow Response  
 363 From Boulder-Induced Geomorphic Changes. *Water Resources Research*, *56*(10), e2020WR027719.
- 364 D'Ippolito, A., Lauria, A., Alfonsi, G., & Calomino, F. (2019). Investigation of flow resistance exerted by rigid  
 365 emergent vegetation in open channel. *Acta Geophysica*, *67*(3), 971-986.
- 366 Ensign, S. H., & Doyle, M. W. (2005). In-channel transient storage and associated nutrient retention: Evidence from  
 367 experimental manipulations. *Limnology and oceanography*, *50*(6), 1740-1751.
- 368 Gooseff, M. N. (2010). Defining hyporheic zones—advancing our conceptual and operational definitions of where  
 369 stream water and groundwater meet. *Geography Compass*, *4*(8), 945-955.
- 370 Grant, S. B., Stewardson, M. J., & Marusic, I. (2012). Effective diffusivity and mass flux across the sediment-water  
 371 interface in streams. *Water Resources Research*, *48*(5).
- 372 Grant, S. B., Stolzenbach, K., Azizian, M., Stewardson, M. J., Boano, F., & Bardini, L. (2014). First-order  
 373 contaminant removal in the hyporheic zone of streams: Physical insights from a simple analytical model.  
 374 *Environmental science & technology*, *48*(19), 11369-11378.
- 375 Huang, S.-H., & Yang, J. Q. (2021). *Experimental data of vegetation-induced hyporheic exchange experiment in*  
 376 *Ecoflume of St. Anthony Falls Laboratory on 2021 (29GB)*. <https://doi.org/10.13020/W282-JJ11>
- 377 Huang, S.-H., & Yang, J. Q. (2022a). *Data of complementary experiments of 'Vegetation-induced hyporheic*  
 378 *exchange experiment in Ecoflume of St. Anthony Falls Laboratory on 2021'* Version 1.0.0).  
 379 <https://doi.org/10.5281/zenodo.6412364>
- 380 Huang, S.-H., & Yang, J. Q. (2022b). *Shih-HsunHuang/Vegetated-induced-hyporheic-exchange* Version v1.1.0).  
 381 <https://doi.org/10.5281/zenodo.6407198>
- 382 Islam, M. R., & Zhu, D. Z. (2013). Kernel density-based algorithm for despiking ADV data. *Journal of Hydraulic*  
 383 *Engineering*, *139*(7), 785-793.

- 384 Jones Jr, J. B., & Holmes, R. M. (1996). Surface-subsurface interactions in stream ecosystems. *Trends in Ecology &*  
 385 *Evolution*, 11(6), 239-242.
- 386 Jørgensen, B. B., & Revsbech, N. P. (1985). Diffusive boundary layers and the oxygen uptake of sediments and  
 387 detritus 1. *Limnology and oceanography*, 30(1), 111-122.
- 388 Lee, A., Aubeneau, A. F., Cardenas, M. B., & Liu, X. (2022). Hyporheic exchange due to cobbles on sandy beds.  
 389 *Water Resources Research*, e2021WR030164.
- 390 Lewandowski, J., Putschew, A., Schwesig, D., Neumann, C., & Radke, M. (2011). Fate of organic micropollutants  
 391 in the hyporheic zone of a eutrophic lowland stream: Results of a preliminary field study. *Science of the*  
 392 *Total Environment*, 409(10), 1824-1835.
- 393 Ma, L., Shi, Y., Siemianowski, O., Yuan, B., Egner, T. K., Mirnezami, S. V., . . . Cademartiri, L. (2019). Hydrogel-  
 394 based transparent soils for root phenotyping in vivo. *Proceedings of the National Academy of Sciences*,  
 395 116(22), 11063-11068.
- 396 Marion, A., Bellinello, M., Guymer, I., & Packman, A. (2002). Effect of bed form geometry on the penetration of  
 397 nonreactive solutes into a streambed. *Water Resources Research*, 38(10), 27-21-27-12.
- 398 McCallum, J. L., Höhne, A., Schaper, J. L., Shanafield, M., Banks, E. W., Posselt, M., . . . Lewandowski, J. (2020).  
 399 A numerical stream transport modeling approach including multiple conceptualizations of hyporheic  
 400 exchange and spatial variability to assess contaminant removal. *Water Resources Research*, 56(3),  
 401 e2019WR024987.
- 402 Nepf, H. M. (1999). Drag, turbulence, and diffusion in flow through emergent vegetation. *Water resources research*,  
 403 35(2), 479-489.
- 404 Nepf, H. M. (2012). Flow and transport in regions with aquatic vegetation. *Annual review of fluid mechanics*, 44,  
 405 123-142.
- 406 Nepf, H. M., & Koch, E. W. K. (1999). Vertical secondary flows in submersed plant-like arrays. *Limnology and*  
 407 *oceanography*, 44(4), 1072-1080.
- 408 O'Connor, B. L., & Harvey, J. W. (2008). Scaling hyporheic exchange and its influence on biogeochemical reactions  
 409 in aquatic ecosystems. *Water Resources Research*, 44(12).
- 410 O'Connor, B. L., & Hondzo, M. (2008). Dissolved oxygen transfer to sediments by sweep and eject motions in  
 411 aquatic environments. *Limnology and Oceanography*, 53(2), 566-578.
- 412 Osenbroch, L. K. H., Hjertager, B. H., & Solberg, T. (2005). Experiments and CFD modelling of fast chemical  
 413 reaction in turbulent liquid flows. *International Journal of Chemical Reactor Engineering*, 3(1).
- 414 Packman, A. I., Salehin, M., & Zaramella, M. (2004). Hyporheic exchange with gravel beds: Basic hydrodynamic  
 415 interactions and bedform-induced advective flows. *Journal of Hydraulic Engineering*, 130(7), 647-656.
- 416 Philippas, D. (2014). Analysis of Covariance (ANCOVA). In A. C. Michalos (Ed.), *Encyclopedia of Quality of Life*  
 417 *and Well-Being Research* (pp. 157-161). Springer Netherlands. [https://doi.org/10.1007/978-94-007-0753-](https://doi.org/10.1007/978-94-007-0753-5_82)  
 418 [5\\_82](https://doi.org/10.1007/978-94-007-0753-5_82)
- 419 Roche, K., Blois, G., Best, J., Christensen, K., Aubeneau, A., & Packman, A. (2018). Turbulence links momentum  
 420 and solute exchange in coarse-grained streambeds. *Water Resources Research*, 54(5), 3225-3242.
- 421 Roche, K. R., Li, A., Bolster, D., Wagner, G. J., & Packman, A. I. (2019). Effects of turbulent hyporheic mixing on  
 422 reach-scale transport. *Water Resources Research*, 55(5), 3780-3795.
- 423 Rousseau, G., & Ancey, C. (2020). Scanning PIV of turbulent flows over and through rough porous beds using  
 424 refractive index matching. *Experiments in Fluids*, 61(8), 1-24.
- 425 Salehin, M., Packman, A. I., & Wörman, A. (2003). Comparison of transient storage in vegetated and unvegetated  
 426 reaches of a small agricultural stream in Sweden: seasonal variation and anthropogenic manipulation.  
 427 *Advances in Water Resources*, 26(9), 951-964.
- 428 Salvador, G. P., Stoesser, T., Rummel, A. C., & Rodi, W. (2007). Turbulent shallow flow through vegetation. Fifth  
 429 International Symposium on Environmental Hydraulics (ISEH V),
- 430 Shen, G., Yuan, J., & Phanikumar, M. S. (2020). Direct numerical simulations of turbulence and hyporheic mixing  
 431 near sediment–water interfaces. *Journal of Fluid Mechanics*, 892.
- 432 Tanino, Y., & Nepf, H. M. (2008). Lateral dispersion in random cylinder arrays at high Reynolds number. *Journal*  
 433 *of Fluid Mechanics*, 600, 339-371.
- 434 Tonina, D., & Buffington, J. M. (2007). Hyporheic exchange in gravel bed rivers with pool-riffle morphology:  
 435 Laboratory experiments and three-dimensional modeling. *Water Resources Research*, 43(1).
- 436 Tonina, D., & Buffington, J. M. (2009). Hyporheic exchange in mountain rivers I: Mechanics and environmental  
 437 effects. *Geography Compass*, 3(3), 1063-1086.
- 438 Voermans, J., Ghisalberti, M., & Ivey, G. (2017). The variation of flow and turbulence across the sediment–water  
 439 interface. *Journal of Fluid Mechanics*, 824, 413-437.

- 440 Voermans, J. J., Ghisalberti, M., & Ivey, G. N. (2018a). A model for mass transport across the sediment-water  
441 interface. *Water Resources Research*, *54*(4), 2799-2812.
- 442 Voermans, J. J., Ghisalberti, M., & Ivey, G. N. (2018b). The Hydrodynamic Response of the Sediment-Water  
443 Interface to Coherent Turbulent Motions. *Geophysical Research Letters*, *45*(19), 10,520-510,527.
- 444 Wohl, E. (2016). Spatial heterogeneity as a component of river geomorphic complexity. *Progress in Physical  
445 Geography*, *40*(4), 598-615.
- 446 Wu, F.-C., Tseng, R.-L., & Juang, R.-S. (2001). Kinetic modeling of liquid-phase adsorption of reactive dyes and  
447 metal ions on chitosan. *Water research*, *35*(3), 613-618.
- 448 Xu, Y., & Nepf, H. (2020). Measured and predicted turbulent kinetic energy in flow through emergent vegetation  
449 with real plant morphology. *Water Resources Research*, *56*(12), e2020WR027892.
- 450 Yang, J. Q., Chung, H., & Nepf, H. M. (2016). The onset of sediment transport in vegetated channels predicted by  
451 turbulent kinetic energy. *Geophysical Research Letters*, *43*(21), 11,261-211,268.
- 452 Yang, J. Q., Kerger, F., & Nepf, H. M. (2015). Estimation of the bed shear stress in vegetated and bare channels  
453 with smooth beds. *Water Resources Research*, *51*(5), 3647-3663.
- 454 Yang, J. Q., & Nepf, H. M. (2018). A turbulence-based bed-load transport model for bare and vegetated channels.  
455 *Geophysical Research Letters*, *45*(19), 10,428-410,436.
- 456 Yang, J. Q., & Nepf, H. M. (2019). Impact of vegetation on bed load transport rate and bedform characteristics.  
457 *Water Resources Research*, *55*(7), 6109-6124.
- 458 Yuan, Y., Chen, X., Cardenas, M. B., Liu, X., & Chen, L. (2021). Hyporheic exchange driven by submerged rigid  
459 vegetation: a modeling study. *Water Resources Research*, *57*(6), e2019WR026675.
- 460 Zhao, M.-d., & Fan, Z.-l. (2019). Emergent vegetation flow with varying vertical porosity. *Journal of  
461 Hydrodynamics*, *31*(5), 1043-1051.
- 462